A Systematic Approach for the Design of UV Reactors Using Computational Fluid Dynamics

B. A. Wols and J. A. M. H. Hofman
KWR Watercycle Research Institute, Water Technology Dept., 3433 PE Nieuwegein, The Netherlands
Delft University of Technology, Civil Engineering Dept., 2600 GA Delft, The Netherlands

E. F. Beerendonk
KWR Watercycle Research Institute, Water Technology Dept., 3433 PE Nieuwegein, The Netherlands

W. S. J. Uijttewaal and J. C. van Dijk
Delft University of Technology, Civil Engineering Dept., 2600 GA Delft, The Netherlands

DOI 10.1002/aic.12255
Published online April 16, 2010 in Wiley Online Library (wileyonlinelibrary.com).

A wide variation exists in the geometries of UV reactors, which results in completely different hydrodynamics and therefore large differences with respect to the disinfection and oxidation performance. Among the large number of reactor types, it is not known beforehand which reactor type has the best performance with respect to disinfection or oxidation, and if such a reactor is the best reactor out of all the possible reactor designs. In this research, a systematic approach for the design of UV reactors is followed that makes use of computational fluid dynamics (CFD) modeling. To that end, the inactivation of Bacillus subtilis *and degradation of atrazine was determined for a wide range of UV systems by means of CFD. The efficacy of UV systems was evaluated and improvements were made by taking measures that increase the mean dose and/or narrow the dose distribution, such as placing mirrors, enhancing the mixing and placing reactors in series.*
 AIChE J, 57: 193–207, 2011
Keywords: UV disinfection, UV oxidation, reactor design, CFD, hydrodynamics, dose distribution

Introduction

The efficacy of UV systems is largely determined by the hydrodynamic processes occurring within the system. The movement of water parcels inside the UV system defines the amount of UV radiation received by these water elements (UV dose). The spatial differences in the UV radiation field and the differences in residence times of the water elements cause a certain distribution of UV doses. From this UV dose distribution, the disinfection and/or oxidation performance is determined. For a proper estimation of the dose distribution in a UV system, knowledge of the transfer and mixing processes is therefore essential. Computational fluid dynamics (CFD) is a powerful tool to simulate these processes.[1–7] In combination with a particle-tracking routine and an irradiation model, the UV dose distribution can be calculated. A similar approach was followed to determine the efficacy of ozone contactors.[8] The CFD calculations are often used as a design tool for UV reactors. Several authors evaluated the disinfection performance of different reactors using CFD.[3,6,7] They found differences in the disinfection performance between the various reactors, which were related to the hydrodynamics of the systems. Modifications to the geometry of the reactor, such as baffle plates or rings, can result in an increase in disinfection capacity.[1,2] For oxidation, the work of Sozzi and Taghipour[9] as well as Alpert et al.[10] can

Correspondence concerning this article should be addressed to B. A. Wols at bas.wols@kwrwater.nl.

be mentioned. These researchers predicted the conversion of chemical compounds in annular reactors by UV in combination with hydrogen peroxide. Sozzi and Taghipour[9] found that the reactor with hydrodynamics closer to a plug flow reactor resulted in a higher conversion of chemical compounds.

A large variation exists in the geometries of UV reactors, which may result in completely different hydrodynamic processes occurring within each system. As a result, the dose distribution, disinfection, and oxidation may be different, even though the flow rate, lamp power, and water absorbance are the same. Among the large number of reactor types, it is not known beforehand which reactor type has the best performance with respect to disinfection or oxidation, and if such a reactor is the best reactor out of all the possible reactor designs. In this research, a systematic approach for the design of UV reactors is followed that makes use of CFD modeling. Also, design aspects such as placing mirrors, determining the lamp size and placing reactors in series are considered. The various designs are subjected to the following criteria: disinfection performance, oxidation performance, and energy consumption. The potential in energy reduction for existing UV reactors and new reactor designs is explored as well. This is the first time such a comprehensive study is made on the design aspects and the performance of a wide range of reactors.

Materials and Methods

Approximation of dose distribution

The dose distribution inside a UV reactor can be approximated by an analytical probability density function. In addition to the CFD predictions, this approach was used to perform a sensitivity analysis with respect to the reaction kinetics. The effect of narrowing the dose distribution on the energy consumption can then be easily explored for different kinetic constants. A (shifted) exponential dose distribution is assumed (Figure 1), which is obtained from an exponential probability density function:

$$f(D) = \lambda \exp(-\lambda(D - D_{\min})) \tag{1}$$

where D represents the UV dose, $D_{\min}$ the shift in dose distribution and λ a distribution factor. The mean dose (D_{mean}) is determined by calculating the expected value (first statistical moment) of the dose from this probability density function:

$$D_{\text{mean}} = \frac{1}{\lambda} + D_{\min}. \tag{2}$$

The dose distribution is characterized by the factor D_{10}/D_{mean} (D_{10} is the 10th percentile of the dose). When D_{10}/D_{mean} equals 1, the system resembles a perfect plug flow with no variations in doses. When D_{10}/D_{mean} is smaller than 1, the hydrodynamics of the system are not optimal, which is denoted as suboptimal hydrodynamics. For a range of D_{10}/D_{mean}, the dose distributions are simulated according to Eq. 1, for which the power is calculated to obtain a certain disinfection or oxidation level. This is calculated as follows: for each value of the factor D_{10}/D_{mean}, a mean dose is calculated that corresponds to the required log removal or log degradation. Should the distribution become wider, a higher mean dose is needed to obtain a similar removal or degradation. It is assumed that the power of the UV lamps scales linearly with the mean dose, so that the energy consumption as a function of the dose distribution (factor D_{10}/D_{mean}) can be determined for each required extent of removal or degradation. This results in the differences in energy consumption as a function of the factor D_{10}/D_{mean}. The calculated energy (E) is normalized with the energy of a perfect plug flow (E_{ideal}), which is defined as the energy consumption at $D_{10}/D_{\text{mean}} = 1$.

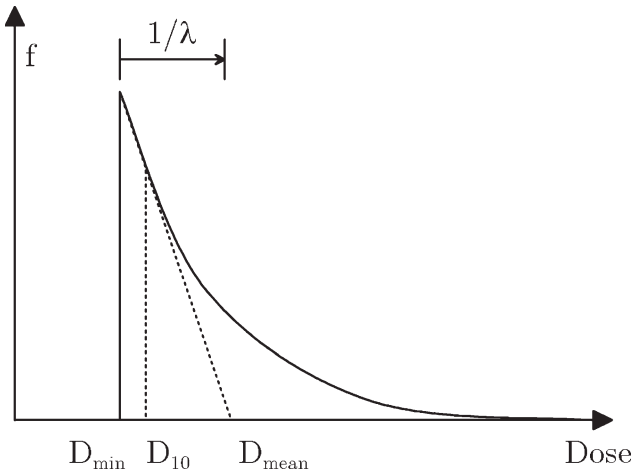

Figure 1. Shifted exponential dose distribution.

Description of CFD model

A finite element package, COMSOL v3.5a, was used for the CFD modeling. The Reynolds averaged Navier–Stokes equations, with a closure given by the equations for the turbulent kinetic energy and turbulent dissipation (k-ε model), were solved using this model. The equations were solved using a direct matrix solver (PARDISO) and convergence was obtained when the relative error on the solution was less than 1E-3. The domain is discretized with tetrahedrons using quadratic finite elements.

We have chosen to use the RANS approach with a k-ε turbulence model, because reasonable results are obtained at acceptable computational costs. Liu et al.[11] showed that the differences in disinfection results between the k-ε model and other turbulence model are within 10%. More advanced CFD model, such as the large-eddy simulation, which accounts for the large-scale turbulent motions varying in time and space, would result in a more accurate solution of the hydrodynamics.[12] However, using a large-eddy simulation for all the reactor designs would be very elaborative and time-consuming, and probably not necessary, because the differences in the performance of the various designs can be clearly shown using the k-ε turbulence model.

In the resolved flow field 4900 particles were released that traced the pathways of the fluid parcels.[13] Particles were assumed to be small enough to move in conjunction with the flow. The particle movements consist of an advection displacement induced by the computed velocity field and a diffusion displacement induced by the turbulent diffusion

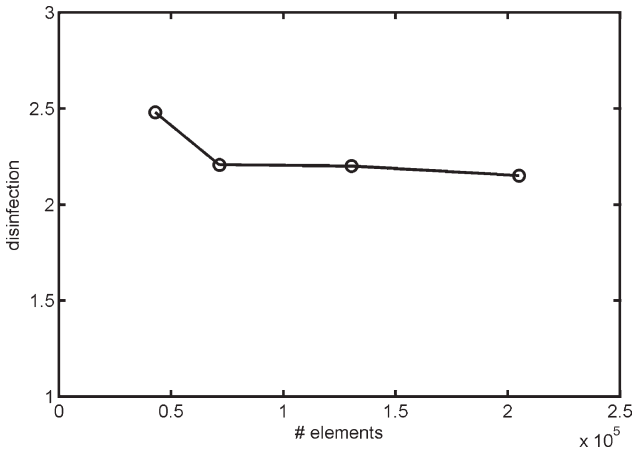

Figure 2. Mesh independency study for the bench-scale reactor.

The predicted disinfection of *B. subtilis* is shown as a function of the number of mesh elements.

coefficient, determined from the k and ε. To account for this latter contribution, a diffusive velocity is constructed by drawing a random variable from a uniform distribution with mean zero and a standard deviation which is in agreement with the turbulent diffusion coefficient. The UV irradiance was calculated by a MSSS model,[14] which divided the UV lamp into 200 segments and calculated the optical pathway and corresponding UV irradiance from each segment of the lamp to each mesh point of the computational domain. The radiation model accounted for refraction and reflection at the interfaces (air-quartz and quartz-water), UV absorbance in quartz and in water and focusing.[14] The UV dose of a particle was calculated by integrating the UV irradiance over the particle's path. The UV dose distribution was determined from the doses of the particles that cross the reactor outlet. The reactor outlet was chosen at a position where the UV irradiance was diminished to zero.

A mesh independency study was performed for the reference bench-scale reactor using four mesh sizes, corresponding to a maximum mesh size (distance between the edge points of a tetrahedral) of 0.02 m, 0.015 m, 0.0125 m, and 0.01 m, respectively (Figure 2). The predicted disinfection results were converged at an amount of ~100,000 elements. Similar mesh sizes were used for the other UV reactors.

Low-pressure lamps that emitted all the UV radiation at a wavelength of 254 nm were chosen. From the UV dose distribution, disinfection was predicted for *Bacillus subtilis*, assuming a delayed Chick–Watson relation: beyond a threshold dose D_0, log inactivation increases linearly with the dose (D). For a dose distribution $f(D)$, the log inactivation DE is calculated by:

$$\mathrm{DE} = -^{10}\log\left(\int f(D)\cdot\exp\left(-k_\mu(D-D_0)\right)dD\right), \quad (3)$$

where k_μ represents the inactivation rate constant (cm^2/mJ). The kinetic constants were obtained from Hijnen et al.[15]

In advanced oxidation processes, hydrogen peroxide is added to the UV reactor. Organic compounds can be degraded by the effect of direct photolysis and/or the reaction with hydroxyl ($OH^\cdot$) radicals. The hydroxyl radicals form when the hydrogen peroxide is irradiated by the UV lamps. The reaction by photolysis for a certain compound N_i (e.g., organic compound or hydrogen peroxide) is given by[16]:

$$\frac{d[N_i]}{dt} = -E_{\mathrm{CFD}}\frac{1-10^{-A}}{A}\Phi_{N_i}\varepsilon_{N_i}[N_i], \quad (4)$$

where Φ represents the quantum yield, ε the molar extinction (L/mol/cm), and A represents the absorption, which can be calculated from the summation of the molar extinction times the concentration over all the compounds in the water ($A = L\sum\varepsilon_{N_i}[N_i]$) or from the 1-cm transmittance (T_{10}) of the water ($A = -^{10}\log(T_{10})$). E_{CFD} is the UV photon flux (mmol/cm^2/s), for which a unit conversion is needed from the UV intensity I (mW/cm^2) as calculated by the CFD model:

$$E_{\mathrm{CFD}} = \frac{I}{N_{\mathrm{A}}E_{\mathrm{f}}}, \quad (5)$$

where E_{f} is the energy of a photon (J) and N_{A} is Avogadro's constant (1/mol).

It is assumed that upstream of the reactor the hydrogen peroxide mixed perfectly with the water. The $OH^\cdot$ radicals react very quickly with different contaminants in the water so that a steady-state concentration of $OH^\cdot$ radicals immediately forms.[16,17] The equilibrium concentration for the $OH^\cdot$ radicals is then calculated by:

$$[\mathrm{OH}^\bullet] = 2E_{\mathrm{CFD}}\frac{1-10^{-A}}{A}\frac{\Phi_{\mathrm{H_2O_2}}\varepsilon_{\mathrm{H_2O_2}}[\mathrm{H_2O_2}]}{\sum k_i[N_i]}, \quad (6)$$

where k_i represents the reaction rate of contaminant i (L/mol/s) with $OH^\cdot$ radicals and $[N_i]$ the concentration of contaminant i (mol/L). The factor two is introduced because two $OH^\cdot$ radicals form when the hydrogen peroxide is irradiated by UV. The factor $\sum k_i[N_i]$ contains the reactions with all the compounds (including peroxide) in the water. Since the number of compounds can be very large, the reactions with the background components in the water were not individually solved for all the background components but treated as one overall reaction with a rate of 20,000 (s^{-1}).

The conversion of a contaminant N_0 by direct photolysis and reaction with $OH^\cdot$ radicals can be written as (where one contaminant reacts with one $OH^\cdot$ radical):

$$\frac{dN_0}{dt} = -E_{\mathrm{CFD}}\frac{1-10^{-A}}{A}\left(\Phi_N\varepsilon_N + 2\frac{\Phi_{\mathrm{H_2O_2}}\varepsilon_{\mathrm{H_2O_2}}[\mathrm{H_2O_2}]}{\sum k_i[N_i]}k_0\right)N_0, \quad (7)$$

which represents a first-order reaction. The reduction of H_2O_2 due to the production of $OH^\cdot$ radicals is assumed to be small, so that the H_2O_2 concentration remains constant in the calculation. Equation 7 is solved over the path of a particle, so that the conversion is calculated for each particle.

An assessment is made of the energy efficacy of several types of UV reactors. The removal of *Bacillus subtilis*, as well as the oxidation of atrazine with an injection of 10 mg/L H_2O_2, is considered for a UV transmittance in water of 80% over 1 cm. All relevant parameters used in the model are given in Table 1. The kinetic parameters for hydrogen

Table 1. Parameters Used for the CFD Calculations

Flow rate	Q (m^3/s)	0.005
Total power UVC (all lamps)	P (W)	Var, 200–2000
Diameter UV lamp	D_{lamp} (m)	Var, ~0.05
Thickness quartz sleeve	d_q (m)	0.0019
Transmittance water	$T_{10,w}$ (%)	80
Transmittance quartz	$T_{10,q}$ (%)	96
Inactivation constant *B. subtilis*	k_μ (cm^2/mJ)	0.136
Threshold inactivation *B. subtilis*	D_0 (mJ/cm^2)	12.3
Initial concentration H_2O_2	C (mg/L)	10
Reaction constant H_2O_2 with $OH^\bullet$	$k_{H_2O_2}$ (L/mol/s)	$2.7 \cdot 10^7$
Reaction constant atrazine with $OH^\bullet$	k_{ATZ} (L/mol/s)	$2.6 \cdot 10^9$
Quantum yield H_2O_2	$\Phi_{H_2O_2}$	0.5
Quantum yield atrazine	Φ_{ATZ}	0.05
Molar adsorption H_2O_2	$\varepsilon_{H_2O_2}$ (L/mol/cm)	18.6
Molar adsorption atrazine	ε_{ATZ} (L/mol/cm)	3860

peroxide were obtained from de Laat et al.,[17] whereas the molar adsorption and quantum yield for atrazine were obtained from Nick at al.[18] and the reaction constant of atrazine with $OH^\cdot$ radicals was obtained from Parsons.[19]

Validation of CFD model

For the reference bench-scale reactor, flow fields were measured to validate the CFD model.[20] In Figure 3, the measured and computed velocities are plotted. The recirculation zones downstream of the lamps were somewhat under predicted by the CFD model. But, more importantly, the main flow regions, which are critical for disinfection due to the lower irradiation levels and high velocities here, were simulated well. The CFD model is therefore used with confidence to assess the efficacy of various UV reactor geometries.

Reactor design

Four groups of reactors were considered (Figure 4): reference reactors, annular reactors, crossflow reactors, and streamlined lamp reactors. The reference reactors were used to show how the commonly used types of reactors perform. The other reactor types include new or existing reactor designs, sorted in a group of annular reactors, crossflow reactors, and streamlined lamp reactors. The last group shows the effect of hydrodynamic measures that optimize the shape of the UV lamp.

Reference reactors

A few full scale reactors were taken as a reference: a four-lamp perpendicular system (geometry taken from Rokjer et al.[21]), a one lamp annular system (VRD8) developed by van Remmen UV Techniek, as well as a four-lamp annular system (VRD50) developed by the same manufacturer. Also, a few UV reactors used in research were simulated and served as reference cases. A bench-scale reactor previously used for validation purposes was simulated.[20] Four UV lamps ($D_{lamp} = 4.7$ cm) were placed perpendicular to the flow in a cylindrical reactor with a diameter of 30 cm. The inflow and outflow pipes have a diameter of 12.5 cm. Since the bench-scale reactor could be further hydrodynamically optimized,[20] an optimized version of the bench-scale reactor was also simulated. Here, the upper and lower extremes of the reactor were cut off, so that the reactor was better streamlined with respect to the inflow and outflow pipes. Also, the lamp positions were changed. The optimized version was further optimized by reducing the lamp diameter to 2.5 cm.

Annular reactors

Some other variants of annular systems were considered for calculation as well. The effect of the lamp diameter was investigated first. A system with a large lamp diameter was considered, one where the irradiation field is more uniformly distributed over the cross-section resulting in a narrower dose distribution. The smaller irradiation levels are compensated by the lower mean velocity in the system. The water flows parallel to the UV lamp. The outer diameter is equal to 0.95 m, whereas the diameter of the lamp equals 0.85 m. So, the distance from the lamp surface to the outer wall is equal to 0.05 m, which was found to be the optimal distance for a transmittance of 80% (Appendix). Also, a system with a smaller lamp diameter was considered, denoted as "annular small." The outer diameter is equal to 0.15 m, whereas the diameter of the lamp equals 0.05 m. Moreover, a helical flow system was considered, where the water is forced to circulate around the UV lamp. The swirling effect was achieved by the asymmetrical inflow and outflow pipes. Lastly, a static mixer with an annular lamp in the middle was considered, denoted as "annular mixer." Oblique baffle plates increase the amount of mixing in the system. For these three annular systems, the effect of a mirror layer on the outer wall was also investigated. Bolton[22] indicated that stainless steel reflected <20% of the radiation in the UVC region, whereas Sommer et al.[23] reported reflection rates of 60–65% for aluminum. So, it was assumed that 50% of the radiation was reflected by the mirror layer, whereas for the other calculation there was no reflection at all.

Crossflow reactors

A number of crossflow systems were also considered. In the first system, denoted as "crossflow," a number of

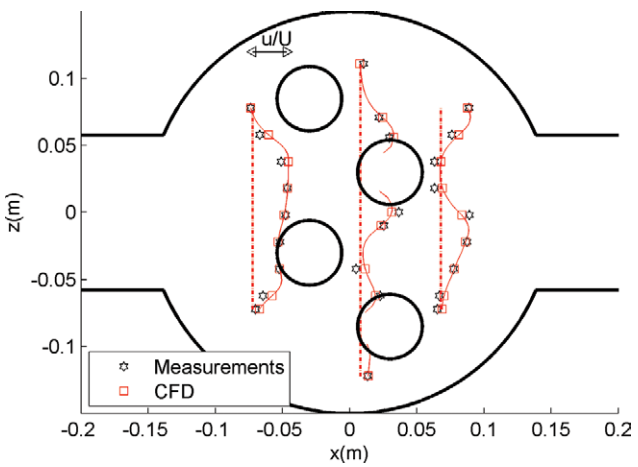

Figure 3. Measured and computed velocities for the bench-scale reactor.

The velocities are normalized with the average velocity in the pipe. [Color figure can be viewed in the online issue, which is available at wileyonlinelibrary.com.]

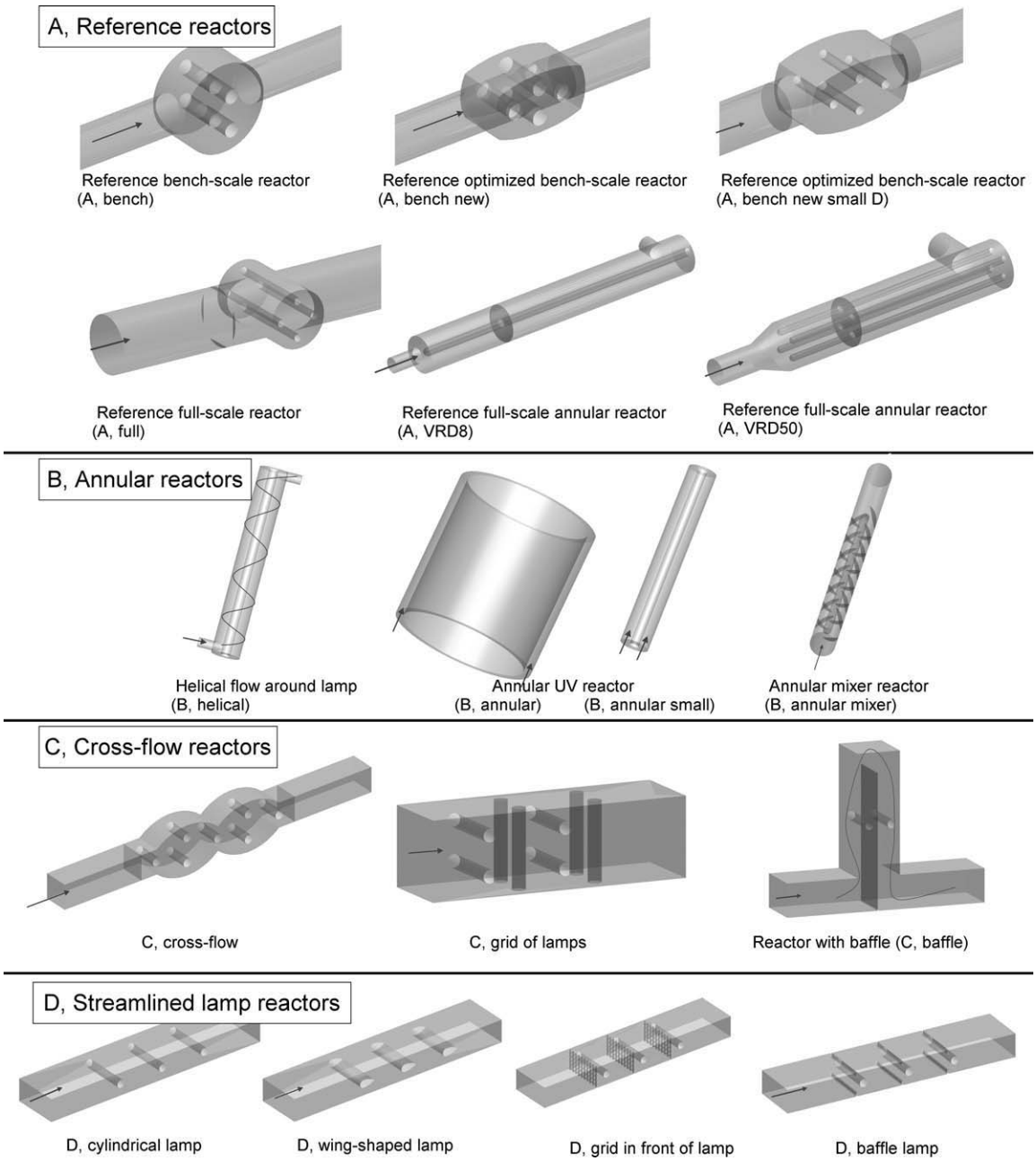

Figure 4. Overview of the geometries of the different UV reactors that were assessed by CFD.

perpendicular lamps were placed at a staggered pattern to force all the water parcels to move close to at least one lamp. The outer geometry of the reactor was chosen such that the distance from the lamp to the wall equals 0.05 m. Also, a system with a grid of lamps ($D_{\text{lamp}} = 0.05$ m) was investigated, denoted as "grid of lamps." Here, the axial direction of the lamp alternated to increase the amount of mixing in the system. The reactor consists of a square duct (0.3 m $\times$ 0.3 m), where the distance between the lamps equals 0.1 m and the distance from the lamp surface to the outer wall again equals 0.05 m. Lastly, a baffle was placed in the middle of the system to force the water to flow closer to the lamps. A lamp ($D_{\text{lamp}} =$ 0.05 m) was placed in each compartment.

Streamlined lamp reactors

In these systems, the effects of measures that optimize the hydrodynamics around a perpendicular UV lamp were investigated. Three UV lamps in a series were considered, each with a diameter of 0.05 m. The distance from the lamp surface to the outer wall was 0.05 m, similar to the annular system. First of all, cylindrical lamps were considered as a reference, denoted as "cylindrical lamp." Second, the cylindrical lamps were replaced by wing-shaped lamps,[12] denoted as wing-shaped lamp. Third, a grid was placed upstream of each lamp to increase the mixing and reduce the wake behind the lamp,[12] denoted as grid in front of lamp. Finally, baffles (height of 0.025 m) were added to force the main

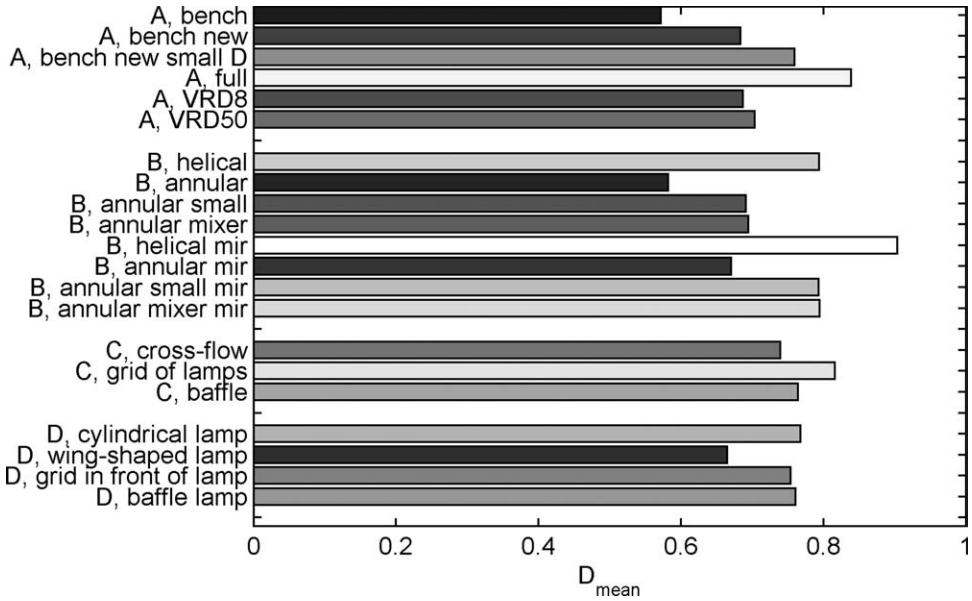

Figure 5. Prediction of the mean dose for all UV reactors by the CFD model.

Mean dose is normalized with a characteristic dose (D_{scale}), explained in Appendix.

flow to move closer to the lamp and increase the mixing, denoted as baffle lamp.

Results and Discussion

The mean UV doses calculated for all reactor types are presented in Figure 5. The mean doses were normalized with respect to a characteristic dose ($D_{scale} = 132$ mJ/cm^2 for a total power of 200 W, explained in Appendix). The mean dose was determined by taking the average dose of all the particles. The values were of the order of 0.55–0.9 of the characteristic dose. So, the amount of radiant energy absorbed by the flow differed up to a factor of 1.5 for the various systems. These differences are caused by: differences in lamp surface area, where radiant energy is lost by reflection and absorption; differences in distances to the outer wall, where radiant energy is lost to the outside of the system; and differences in hydrodynamics. For the reference systems (group A), the modifications to the bench-scale reactor by cutting off the upper and lower parts, as well as reducing the lamp diameter, resulted in an increase in mean dose. The full-scale reactor showed a large mean dose, whereas the full-scale annular reactors (VRD8 and VRD50) had a smaller one. For the annular systems (group B), the helical system had the largest mean dose, indicating that the energy transfer from the lamp to the water was most efficient here. Because of the high mixing and helical flow patterns, no short-circuit flows with high velocities and low doses were present here, resulting in a high-mean dose. Increasing the lamp diameter for the parallel flow system resulted in lower irradiation levels in the water, so that the mean dose was smaller. Placing mirrors on the side walls (50% reflection) yielded an increase in the mean dose of around 15%. For the crossflow systems (group C), mean doses were in general higher than for the annular systems without reflection. The streamlined lamp systems (group D) also showed high-mean doses, except for the wing-shaped system, where less energy was transferred due to the larger lamp area.

• The results of all the UV systems are summarized in Figure 6, where the dose distribution for each system is plotted. Although the lamp power and therefore the doses are much higher for oxidation, the (normalized) dose distribution is similar for oxidation and disinfection. Also, the normalized mean and minimal doses, the log inactivation of *B. subtilis* (DE) as well as oxidation of atrazine (OX) are given (the UVC power output was set to 200 W for disinfection and to 2000 W for oxidation). The dose of the particle with the lowest dose defined the minimal dose. In Figure 7, the disinfection and oxidation results for each reactor are plotted as well. The various UV reactors showed the following results:

• In Figures 6a–f (Group A), the reference bench-scale reactor showed a peak in the dose distribution at a small dose, which were caused by the short-circuit flows that moved in between the lamps, resulting in small inactivation levels. The geometric modifications to the bench-scale reactor reduced the short-circuit flows (particles with high velocities that had moved in between the lamps) and resulted in a shift of the peak in the dose distribution toward a higher dose. The reference full-scale reactor showed high-oxidation levels as well as high-disinfection levels, mainly because of the high-mean dose. For the annular reference systems, the four-lamp system (VRD50) showed a narrower dose distribution than the one-lamp system (VRD8), because the UV irradiance field is more uniform for the four lamp system. The disinfection levels for this system were the highest of all the reference systems.

• For the annular systems (group B, Figures 6g–j), the annular mixer and helical system showed a nearly symmetrical dose distribution. These systems showed the best oxidation results. The high intensity of mixing in the annular mixer system had resulted in a very narrow dose distribution.

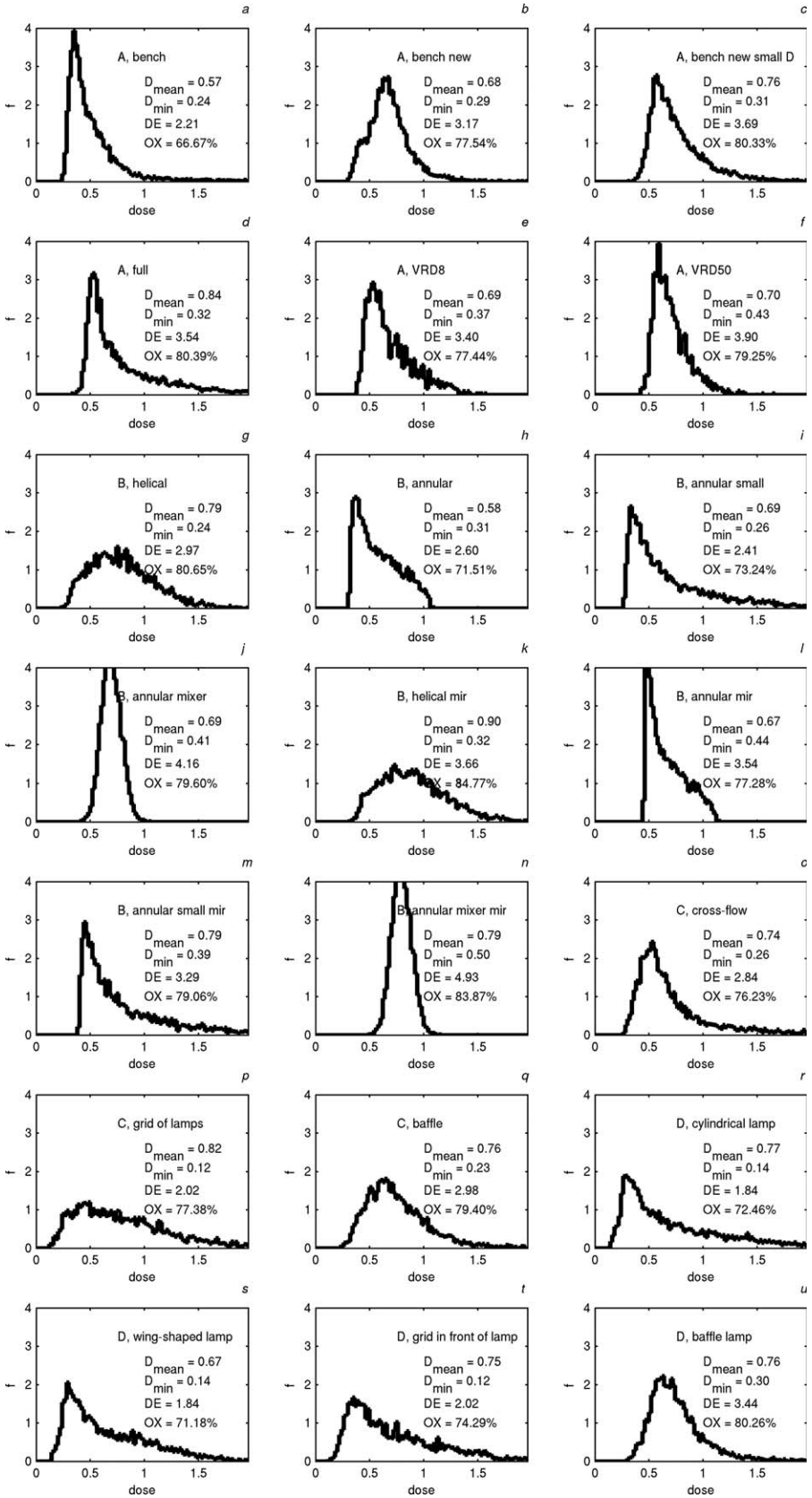

Figure 6. Dose distributions (normalized) for the different reactor designs.

Parameters shown are the normalized mean dose (D_{mean}), normalized minimum dose (D_{min}), log inactivation of *B. subtilis* (DE) and oxidation of atrazine (OX).

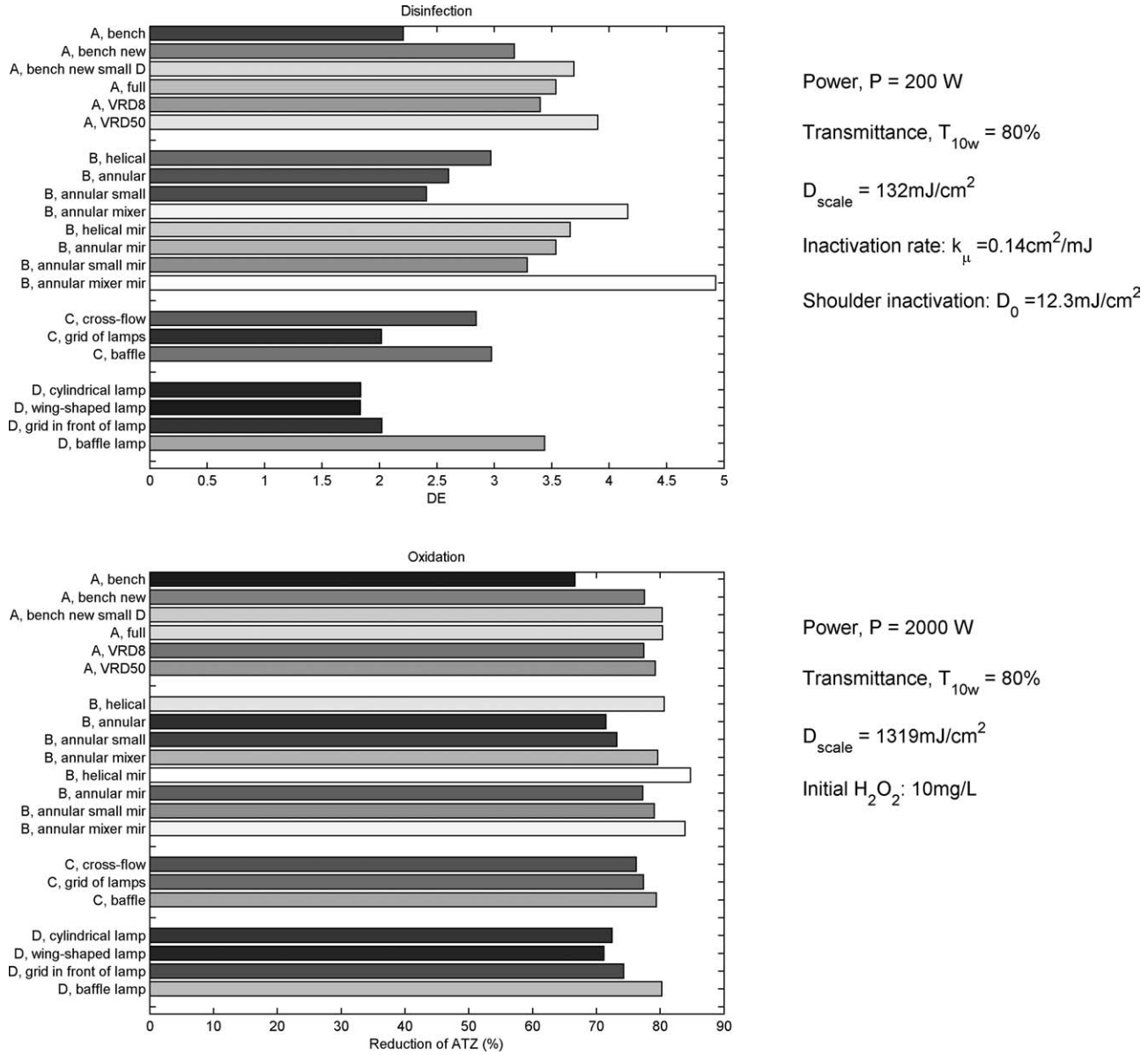

Figure 7. Prediction of the disinfection of *B. subtilis* (upper panel) and oxidation of atrazine in combination with peroxide (lower panel) for each UV reactor.

Consequently, this system showed the highest disinfection results. The other annular system had asymmetrical dose distributions with a peak at the lower dose part. The peak was related to the particles traveling close to the outer wall of the reactor. The annular system with the large lamp diameter showed a smaller dose distribution than the system with a small lamp diameter, as expected, however the mean dose was smaller, because more UV radiation was lost due to the larger quartz sleeve. The overall effect of increasing the lamp diameter was a slightly better disinfection, but a smaller oxidation performance.

• Placing mirrors at the outer walls (Figures 6k–n), such that 50% of the UV radiation is reflected, shifted the peak in the dose distribution toward to higher UV dose levels. Since the reflected radiation had the greatest contribution near the outer wall, where the particles with the lowest doses were located, the smallest doses greatly increased. As a consequence, the disinfection and oxidation performance increased considerably. The annular mixer system with a mirror showed the best disinfection performance of all the systems, whereas the annular helical system and the mixer system showed the best oxidation performance.

• For the crossflow systems (group C, Figures 6o–q), the oxidation levels were predicted high because the mean doses were high. However, the dose distributions were very wide, because a part of the bulk flow moved through areas with much lower irradiation levels than the levels close to the lamp. As a result, especially for the grid of lamps, the disinfection levels were predicted low.

• For the streamlined lamp systems (group D, Figures 6r–u), the reactor containing the cylindrical lamps had a large peak at the smaller doses, so that the disinfection performance was very low. The peak in the dose distribution at the lower

Table 2. Overview of the Results of the Disinfection and Oxidation for the Best Design of Each UV Reactor Group

Group	Best Design	Disinfection *B. subtilis* (Log Inactivation)	Oxidation Atrazine (%)
Reference	A, VRD50	3.90	79
Annular	B, annular mixer	4.16	80
Annular mirror	B, annular mixer mirror	4.93	84
Crossflow	C, baffle lamp	2.98	79
Streamlined lamp	D, baffle	3.44	80

doses was caused by the particles traveling close to the outer walls. The low-irradiation levels in combination with high velocities near the outer walls resulted in low doses. The oxidation results were reasonably good because the mean doses were high. The peak in the dose distribution could not be reduced by changing the lamp to a wing-shaped lamp. Placing a grid in front gave a small reduction in the peak of the dose distribution, so that the disinfection was slightly increased. Adding baffles close to the lamps had a major impact: the dose distribution became more symmetrical and the peak shifted toward a higher dose. The baffles forced the particles to move closer to the lamp, so that the particles close to the outer wall responsible for the low doses would receive higher doses. As a result, log inactivation was almost doubled.

An overview of the disinfection and oxidation results of the best performing reactor in each group is shown in Table 2. The reference systems performed well, because they were already a result of hydrodynamic optimizations, which are clearly visible for the bench-scale reactor, where the modifications had resulted in an increase in inactivation levels of almost 100%. But still the annular mixer showed a big improvement in disinfection performance with respect to the reference systems. By placing a mirror at the outer wall, the disinfection performance was even higher. For the removal of chemical compounds, differences between the systems were less pronounced because oxidation appeared to be less sensitive to the dose distribution. But still the annular mixer showed an improvement for the degradation of chemical compounds.

The results of the disinfection and oxidation predictions are plotted against the mean dose and the 10th percentile of the dose (D_{10}) in Figure 8. The D_{10} characterizes the low dose part of the distribution better than the minimal dose because it accounts for the skewness of the dose distributions. A strong correlation between the D_{10} and the disinfection ($R^2 = 0.99$) was observed, showing that the D_{10} largely determined the disinfection. The slope of the fit matched with the inactivation constant of *B. subtilis* used here. The correlation between the mean dose and the disinfection was weak ($R^2 = 0.07$). For oxidation both the D_{10} as the mean dose showed a moderate correlation with the degradation.

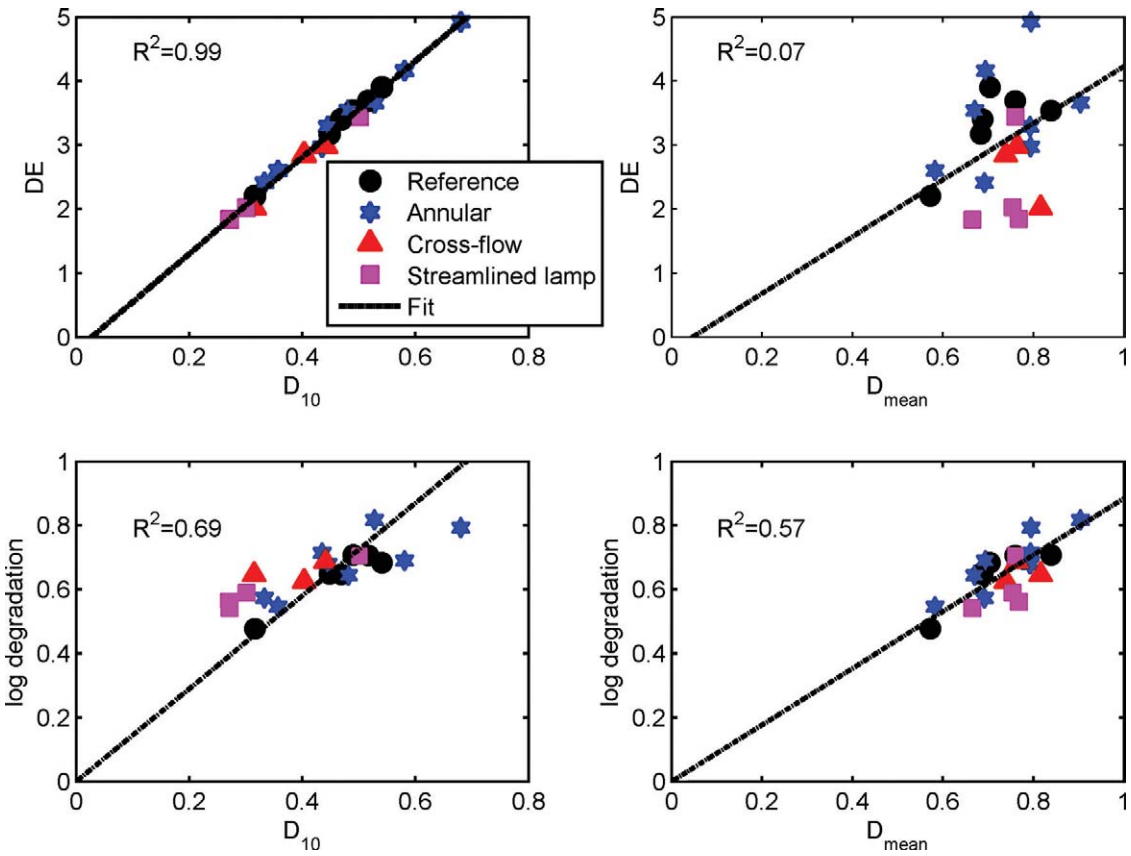

Figure 8. Disinfection and oxidation results as a function of D_{10} (dose at which 10% of the particles has a lower value) and D_{mean} for each UV reactor.

D_{10} and D_{mean} were normalized with the characteristic dose. [Color figure can be viewed in the online issue, which is available at wileyonlinelibrary.com.]

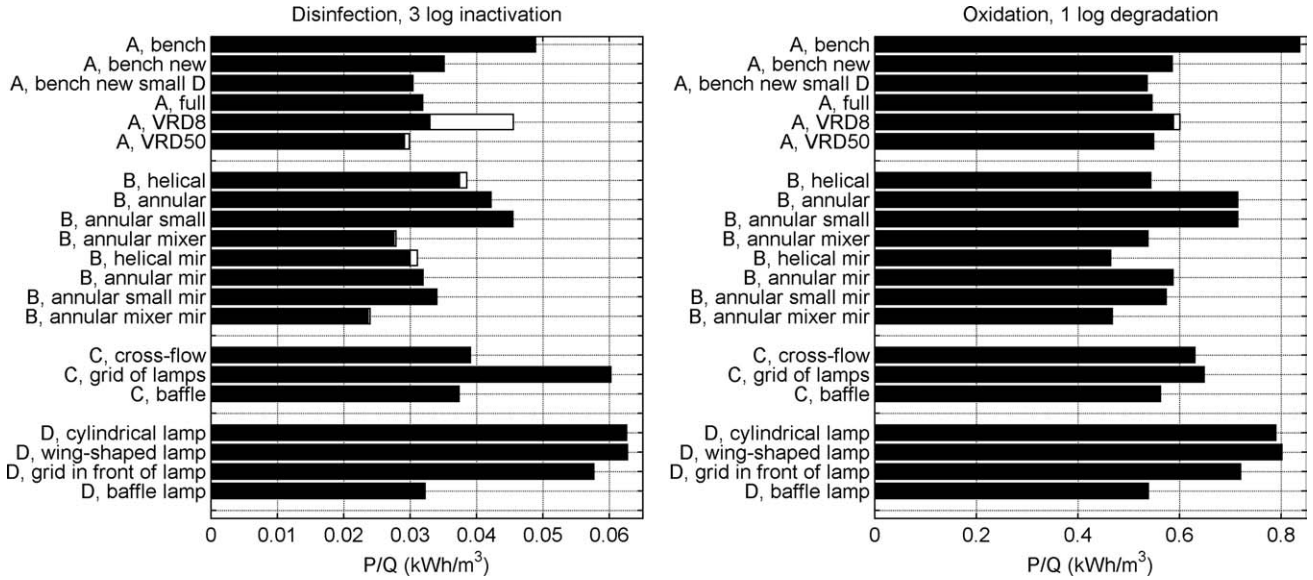

Figure 9. Electrical energy consumption by UV lamps (black bar) and hydraulic losses (white bar) needed to obtain 3 log disinfection of *B. subtilis* (left) or 1 log degradation of atrazine (right).

The white bars are in some cases very small (not visible), indicating that the hydraulic loss is negligibly small.

The differences between oxidation and disinfection are mainly related to the extent of removal. For disinfection, the removal of microorganisms reaches values between 99% (log 2) and 99.999% (log 5), which means that the lower doses are very critical for disinfection. For oxidation, the removal of organic compounds reaches values between 60 and 85%, which are less sensitive to lower doses.

The total use of electrical energy is shown in Figure 9. The energy consumption consists of an electrical energy use by the UV lamp (assuming an efficiency of the lamp of 30%) and a hydraulic loss (assuming a pump efficiency of 50%). The differences in hydraulic energy losses between the systems were large, which was mainly caused by the differences in velocities. For the VRD8 reactor, for example, a higher flow rate was applied than the design conditions of the reactor would allow. To that end, maximum velocities of around 4 m/s occurred in the holes of the baffle plate, so that the pressure loss was very high. Under the design conditions, pressure losses will be comparable with the VRD50 system. The inflow conditions in the helical flow reactor (A, helical) were responsible for a large pressure loss due to a sudden lateral expansion. In general, for disinfection, the hydraulic losses were small with respect to the lamp power. For oxidation, the hydraulic losses were negligibly small

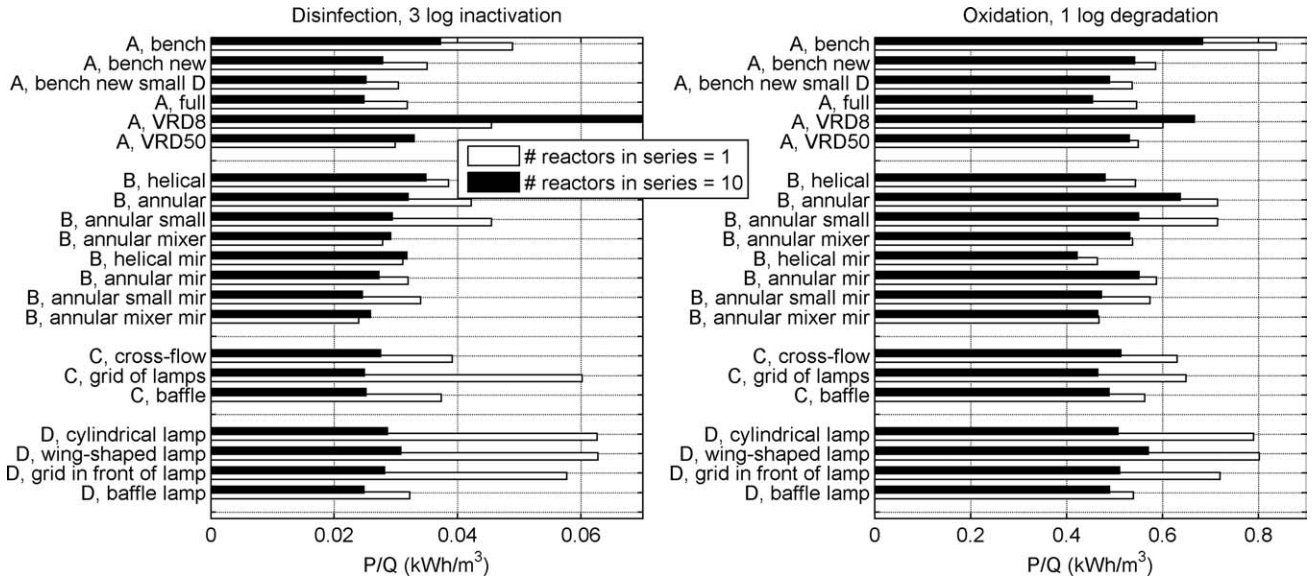

Figure 10. Total energy consumption needed to obtain 3 log disinfection of *B. subtilis* (left) or 1 log degradation of atrazine (right) for one reactor and 10 reactors in series.

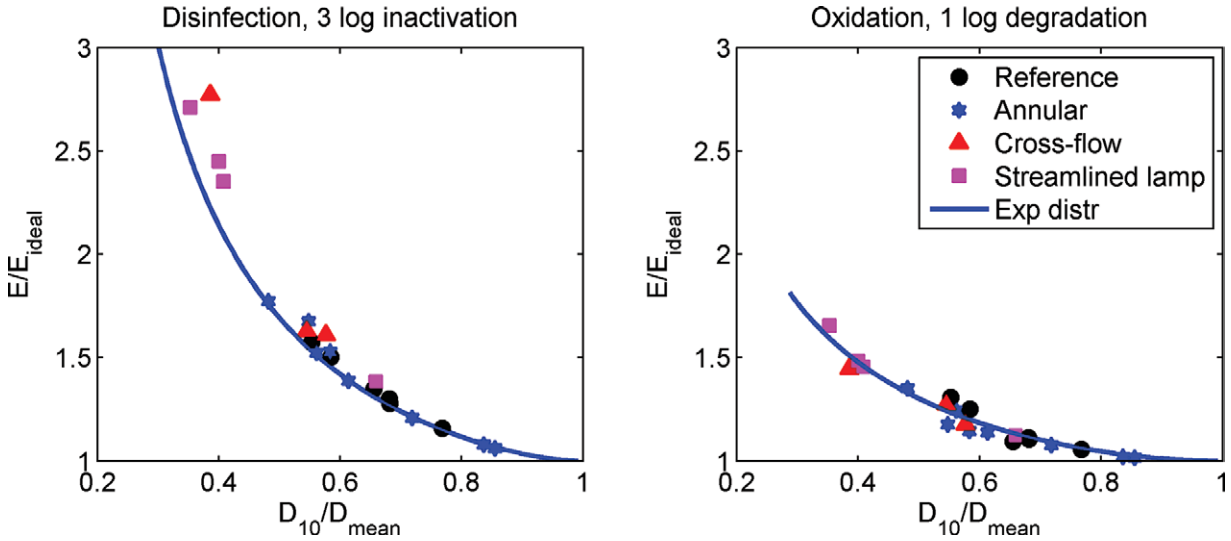

Figure 11. Energy consumption is plotted against the dose distribution.

The energy consumption is shown as the calculated energy E divided by the E_{ideal} in the case of perfect hydrodynamics. The dose distribution is characterized by the 10th percentile dose divided by the mean dose. [Color figure can be viewed in the online issue, which is available at wileyonlinelibrary.com.]

with respect to the high-lamp power. So, the total power consumption is lowest for the annular mixer system.

Another method of optimizing UV systems is placing a number of reactors in series. The radiant power for the system with n reactors in series is reduced by a factor of n in comparison with the system with one reactor. In between each reactor in series, a static mixer is assumed, so that the particles are redistributed over the cross-section. According to the central limit theorem, the dose distribution becomes smaller and approaches closer to the normal distribution after each reactor. As a consequence, the disinfection and oxidation results of the system must increase. However, the hydraulic losses will also increase by a factor of n. The total energy consumption needed to obtain 3 log inactivation of *B. subtilis* or 1 log degradation of atrazine is therefore plotted in Figure 10 in the case of $n = 1$ and $n = 10$. For disinfection, the differences in energy consumption between the systems became smaller when a number of reactors were placed in series. The systems with suboptimal hydrodynamics (such as "A, bench" or "D, cylindrical lamp") had improved considerably. However, the systems with optimal hydrodynamics (such as "B, annular mixer" or "B, helical mir") did not show an improvement because the disinfection was slightly increased by placing reactors in series, whereas the hydraulic power losses were increased as well. For oxidation, the relative gain in energy consumption by placing 10 reactors in series was less than for disinfection, but the absolute gain in energy was much higher. For almost all the systems, the energy consumption can be improved by placing reactors in series because the hydraulic power losses are negligibly small (except for the "A, VRD8").

In Figure 11, the factor E/E_{ideal}, interpreted as the additional energy needed to obtain the same log inactivation or degradation as for the ideal situation, is plotted against D_{10}/D_{mean} using the analytical dose distribution from Eq. 1. The ideal energy consumption is calculated from the mean dose, by assuming that all the particles received the mean dose. The kinetic constants given in Table 1 were used. The values of the additional energies calculated from the dose distributions of the CFD calculations are plotted as well. These values coincide well with the analytical model derived from the exponential dose distribution for disinfection as well as oxidation. So, the exponential dose distribution as described in Eqs. 1 and 2 can be used to predict the energy consumption of a UV system. In this way, the analytical model forms an easy tool to investigate the energy reduction that could be obtained when the D_{10}/D_{mean} is increased. Moreover, it allows for prediction of the sensitivity of the energy reduction with respect to the kinetic constants. The maximum energy reduction is obtained when the dose distribution is reduced to $D_{10} = D_{mean}$. The figure clearly indicates the potential in reduction of energy for the various systems. The annular mixer system showed an E/E_{ideal} close to 1, so that this system is hydrodynamically almost perfect: little reduction in energy can be obtained by further reducing the dose distribution. The D_{10} for existing UV reactors was of the order of 0.5–0.75 of the mean dose, so that a hydrodynamic optimization would result in an energy reduction from 15–50% for disinfection. For one of the reference systems (VRD50), the hydrodynamics were close to the ideal situation (D_{10}/D_{mean} of around 0.75), so that the potential in reduction of energy is small (maximum of 15%). For other systems with a D_{10}/D_{mean} of around 0.5, the energy reduction induced by hydrodynamic optimizations may be larger.

We could, for example, assume that optimizing the hydrodynamics of a UV reactor by modifying the geometry may result in a narrowing of the dose distribution from $D_{10} = 0.5$ D_{mean} to $D_{10} = 0.75$ D_{mean}. This optimization results in a reduction of energy, which is represented as a percentage of the energy consumption before the optimization (Figure 12). Three parameters are distinguished that influence this energy reduction:

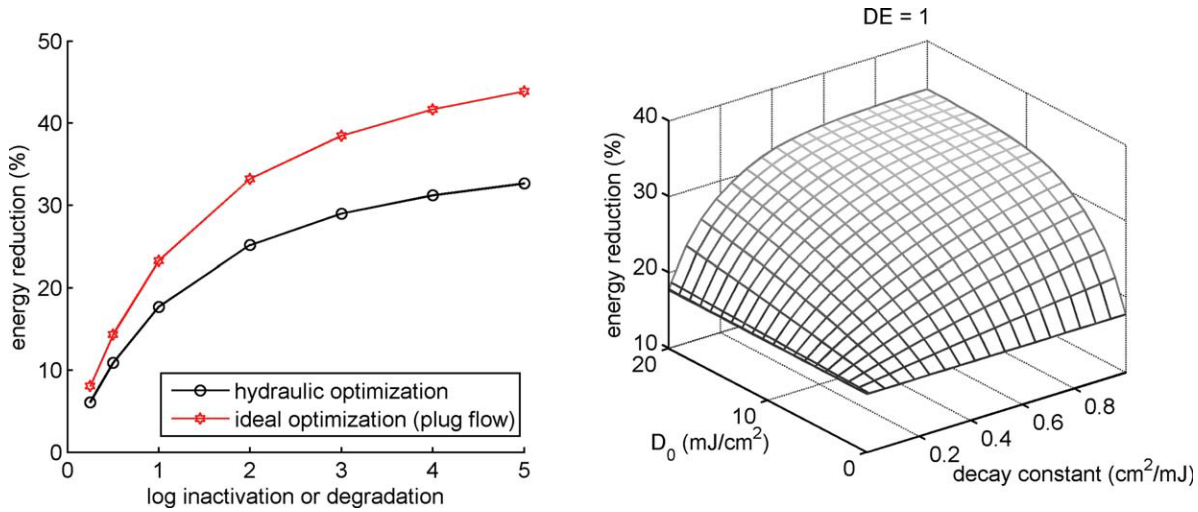

Figure 12. Energy reduction as a function of required log inactivation or degradation (on the left), decay constant and threshold dose (on the right) in the case of the dose distribution being narrowed from D_{10}/D_{mean} = 0.5 to D_{10}/D_{mean} = 0.75.

[Color figure can be viewed in the online issue, which is available at wileyonlinelibrary.com.]

• The total extent of removal. In Figure 12 on the left, the energy reduction that occurs by optimizing the hydrodynamics is plotted as a function of the required log removal or degradation. At a higher required extent of removal, a higher percentage in energy reduction can be obtained because the differences in doses have a greater effect. Since the energy consumption is also higher at a higher log removal, the absolute reduction in energy by a hydrodynamic optimization is then even higher.

• The first-order decay constant, which can be derived from Eq. 3 for disinfection and Eq. 7 for oxidation. In Figure 12 on the right, the energy reduction is plotted as function of the first-order decay and threshold dose for a total removal of log 1. For this fixed extent of removal, the energy reduction does not depend on the decay coefficient when the threshold dose is equal to zero. But in the case of a threshold dose, the energy reduction increases at higher decay constants, because a lower mean dose is needed to obtain the required amount of removal, so that the threshold dose has a bigger impact.

• The threshold dose, which only applies to the disinfection of a small number of microorganisms. At higher threshold doses, the energy reduction obtained from optimizations increases (Figure 12 on the right) because the lower doses are even more critical for disinfection, so that a reduction of these low doses is more effective.

Design considerations

The combination of particle positions and particle velocities determine the dose distribution. The particle positions determine the amount of UV radiation that is received by the particle, which can differ largely due to the large spatial differences in UV radiation field. So, the weak points in the UV systems were related to the parcels of water that travel at the greatest distance from the lamps. At these locations,

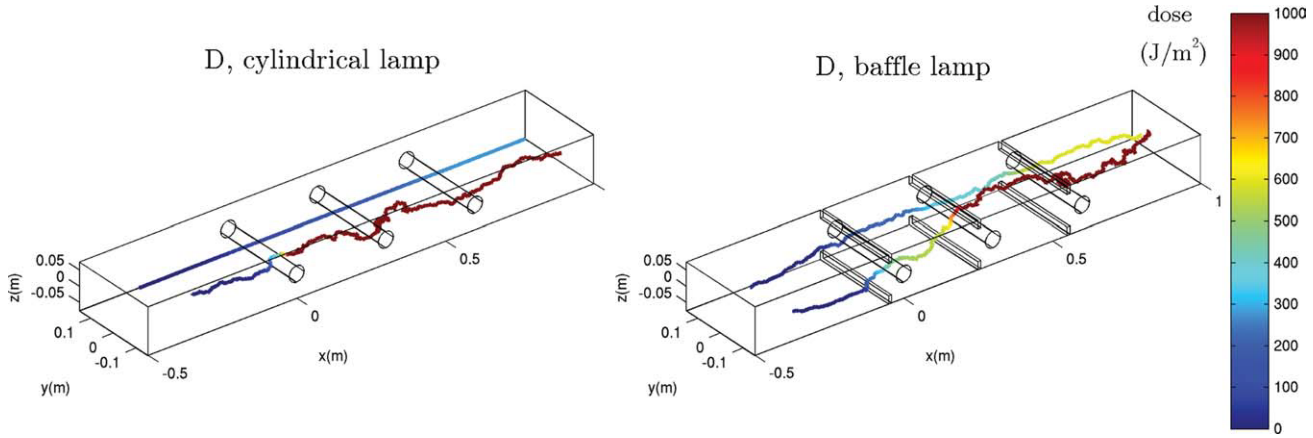

Figure 13. Particle paths inside the UV systems.

The dose received by a particle during its path through the reactor is indicated by the color. The particles with the lowest dose and highest dose are shown. [Color figure can be viewed in the online issue, which is available at wileyonlinelibrary.com.]

usually close to the walls, irradiation levels were low due to absorption of UV radiation in water. For example, the weak points in the annular system were related to the particles that remained close to the outer wall. The system with a helical flow around the lamp or annular mixer therefore had a higher disinfection efficacy due to increased mixing. As a result, particles with low doses did not remain at the outer wall, but also traveled closer to the lamp surface. For the crossflow system, particles traveling close to the outer wall were also responsible for the low-disinfection levels. The effect of the baffles is illustrated in Figure 13, where the particles traveling close to the outer walls were forced to move closer to the lamp. For the same reason, the UV system with alternating lamp orientations showed a wide-dose distribution, caused by the particles that remained in the corners of the reactor. The optimized bench-scale reactor showed good results because the staggered lamp positions forced all the parts of the flow to travel close to at least one lamp. For a good reactor design, it is therefore important that all the particles reach the area close to the lamps. This can be achieved by increasing the mixing in the system and/or by manipulating the main flow, such as placing baffles. The mirrors used in the annular systems resulted in a significant increase in disinfection and oxidation, because the irradiance level at the outer wall was increased by 50% (in the case of 50% of mirroring). The particles with low doses that had moved along the outer wall mainly showed an increase in UV dose.

The effect of increasing the radius of the lamp is ambiguous: on the one hand, the irradiation field was more uniform, so that the dose distribution was narrower; on the other hand, the UV irradiance was lower, so that the mean dose was reduced. For the annular system, the overall effect of increasing the lamp diameter was positive for the disinfection capacity. However, for the bench-scale reactor, the effect was the opposite: the system with the larger lamp diameter predicted a lower disinfection.

Conclusions

A systematic approach for the design of UV reactors is followed that makes use of CFD modeling. To that end, the disinfection performance, oxidation performance, and energy consumption of a wide range of UV reactors was assessed.

The dose distribution is the main parameter that determines the performance of UV reactors. The transfer and (turbulent) mixing processes largely define the dose distribution. By assuming a (shifted) exponential dose distribution, narrowing the dose distribution may lead to a reduction in energy consumption of the order of 20–30%. In other words, the hydrodynamic processes inside the system may largely influence energy consumption. The total reduction in energy depends on the kinetic parameters and the required extent of removal. At a higher extent of removal, the removal is more sensitive to the dose distribution (the low-dose range limits the total removal), so that the difference between good and bad designs becomes more apparent. Since the degradation demands are less severe than the disinfection demands, the energy reduction in terms of percentage was lower for oxidation purposes. The high-energy consumption for the degradation of organic compounds, however, results in a higher energy reduction in absolute terms. So, modifications to the system that narrow the dose distribution are thus attractive for disinfection as well as oxidation. Different UV systems were simulated by the CFD model to assess disinfection and oxidation results for different reactor geometries. By using CFD models, large numbers of reactor geometries can be modeled and, if used with competence, reliable results can be obtained. Although the input parameters such as lamp power, flow rate, and water transmittance were the same, the dose distributions differed greatly for the various UV systems. Hence, the differences between the disinfection levels predicted by the CFD model were large. The 10th percentile of the dose (D_{10}) seemed to be a good characterization of the dose distribution, since it correlates well with the predicted disinfection of all the reactors. The D_{10} for existing UV reactors was of the order of 0.5–0.75 of the mean dose, so that a hydrodynamic optimization would result in an energy reduction from 15 to 50% for disinfection. An annular system, designed as a static mixer with a lamp in the middle, showed a very narrow dose distribution, which comes close to the perfect hydrodynamic system (within 10% of the energy consumption of the ideal system). From the large number of CFD calculations, general design considerations can be drawn. The efficacy of UV systems can be improved by taking measures that increase the mean dose and/or narrow the dose distribution:

Place mirrors at the outer walls, especially in the case of an annular system, which leads to a significant increase in the mean dose and therefore in disinfection and oxidation levels.

Enhance the mixing inside the system to ensure that all the microorganisms come close to the lamps and the dose distribution becomes narrower. This can be achieved by placing baffles or by forcing a helical flow around the lamp.

Place a number of reactors in series with a static mixer in between the reactors to narrow the dose distribution.

Other design considerations are the orientation and size of the lamps. From the simulations, there was a slight preference found for an annular system but no clear preference for the size of the lamp. Although some general design rules can be formulated, due to the complexity of the flow fields and large spatial differences in UV irradiation, CFD is an essential tool to optimize a UV reactor.

Acknowledgments

This work was performed in the TTIW-cooperation framework of Wetsus, centre of excellence for sustainable water technology (www.wetsus.nl) and this work is supported by the joined Dutch Water Supply Companies. Wetsus is funded by the Dutch Ministry of Economic Affairs. The authors thank the participants of the research theme "clean water technology" for the fruitful discussions and their financial support. They also thank van Remmen UV Techniek for allowing the use of the properties of their UV reactors for the CFD calculations.

Literature Cited

1. Blatchley ER III, Do-Quang Z, Janex ML, Laine JM. Process modeling of ultraviolet disinfection. *Water Sci Technol*. 1998;38:63–69.
2. Chiu K, Lyn DA, Savoye P, Blatchley ER. Effect of UV system modifications on disinfection performance. *J Environ Eng*. 1999; 125:459–469.
3. Wright NG, Hargreaves DM. The use of CFD in the evaluation of UV treatment systems. *J Hydroinform*. 2001;3:59–70.

4. Munoz A, Craik S, Kresta S. Computational fluid dynamics for predicting performance of ultraviolet disinfection—sensitivity to particle tracking inputs. *J Environ Eng Sci*. 2007;6:285–301.
5. Ducoste J, Linden K, Rokjer D, Liu D. Assessment of reduction equivalent fluence bias using computational fluid dynamics. *Environ Eng Sci*. 2005;22:615–628.
6. Sozzi DA, Taghipour F. UV reactor performance modeling by Eulerian and Lagrangian methods. *Environ Sci Technol*. 2006;40: 1609–1615.
7. Pan H, Orava M. Performance evaluation of the UV disinfection reactors by CFD and fluence simulations using a concept of disinfection efficiency. *J Water Supply Res Technol*. 2007;56:181–189.
8. Wols BA, Uijttewaal WSJ, Rietveld LC, Stelling GS, van Dijk JC, Hofman JAMH. Residence time distributions in ozone contactors. *Ozone: Sci Eng*. 2008;30:49–57.
9. Sozzi DA, Taghipour F. The importance of hydrodynamics in UV advanced oxidation reactors. *Water Sci Technol*. 2007;55:53–58.
10. Alpert SM, Knappe D, Ducoste J. *The Use of Computational Fluid Dynamics (CFD) to Model UV-Initiated Advanced Oxidation Processes*. Los Angeles: 2007 World Congress on Ozone and Ultraviolet Technologies, 2007.
11. Liu D, Wu C, Linden K, Ducoste J. Numerical simulation of UV disinfection reactors: evaluation of alternative turbulence models. *Appl Math Model*. 2007;31:1753–1769.
12. Wols BA, Uijttewaal WSJ, Rietveld LC, Hofman JAMH, van Dijk JC. *Hydraulic Optimization of a Single UV Lamp Placed Perpendicular to the Flow Direction by Experimental and Numerical Techniques*. Tokyo, Japan: I0$_3$A 19th World Congress, 2009.
13. Wols BA, Hofman JAMH, Uijttewaal WSJ, Rietveld LC, Stelling GS, van Dijk JC. A particle tracking technique to estimate disinfection efficacy in drinking water treatment plants. In: *6th International Conference on CFD in Oil and Gas, Metallurgical and Process Industries*. Trondheim, Norway: SINTEF, NTNU, 2008.
14. Liu D, Ducoste JJ, Jin S, Linden K. Evaluation of alternative fluence rate distribution models. *J Water Supply Res Technol - Aqua*. 2004;53:391–408.
15. Hijnen WAM, Beerendonk EF, Medema GJ. Inactivation credit of UV radiation for viruses, bacteria and protozoan (oo)cysts in water: a review. *Water Res*. 2006;40:3–22.
16. Sharpless CM, Linden KG. Experimental and model comparisons of low- and medium-pressure Hg lamps for the direct and H_2O_2 assisted UV photodegradation of *N*-nitrosodimethylamine in simulated drinking water. *Environ Sci Technol*. 2003;37:1933–1940.
17. de Laat J, Gallard H, Ancelin S, Legube B. Comparative study of the oxidation of atrazine and acetone by H_2O_2/UV, Fe(III)/UV, Fe(III)/H_2O_2/UV and Fe(II) or Fe(III)/H_2O_2. *Chemosphere* 1999;39: 2693–2706.
18. Nick K, Schoeler HF, Mark G, Soylemez T, Akhlaq MS, Schuchmann H-P, von Sonntag C. Degradation of some triazine herbicides by UV radiation such as used in the UV disinfection of drinking water. *J Water Supply Res Technol - Aqua*. 1992;41:82–87.
19. Parsons S. *Advanced Oxidation Processes for Water and Wastewater Treatment*. London, England: IWA Publishing, 2004.
20. Hofman JAMH, Shao L, Wols BA, Uijttewaal WSJ, IJpelaar G. Design of UV reactors by CFD: model development and experimental validation. In: *Proceedings of the European COMSOL Conference*. Grenoble, 2007.
21. Rokjer D, Matthew V, Keesler D, Boryskowsky M, Ducoste J. Medium pressure UV reactor models for validation purposes. In: *Proceedings of the American Water Works Association Water Quality Technology Conference*. Philadelphia, 2003.
22. Bolton JR. Calculation of ultraviolet fluence rate distributions in an annular reactor: significance of refraction and reflection. *Water Res*. 2000;34:3315–3324.
23. Sommer R, Cabaj A, Haider T. Microbicidal effect of reflected UV radiation in devices for water disinfection. *Water Sci Technol*. 1996; 34:173–177.

Appendix

Characteristic dose

A scale factor for the mean dose is introduced to characterize all the reactors and give an indication of the average dose that could be obtained for a reactor with a certain flow rate, lamp power, and water absorbance. The calculation is based upon an annular system. The lamp radius (r_{lamp}) corresponds to the distance from the center of the lamp to the quartz sleeve. The distance (R) is the distance from the quartz sleeve to the outer wall of the reactor. A fixed flow rate Q is fed into the system, so that the mean velocity (U) yields:

$$U = \frac{Q}{\pi\left(2r_{\text{lamp}}R + R^2\right)} \tag{A1}$$

The irradiance field I as a function of radius r is given by (for a 2D system):

$$I(r) = \frac{P_0}{2\pi r} e^{-\alpha\left(r - r_{\text{lamp}}\right)} \tag{A2}$$

where P_0 is the power of the lamp per unit length (W/m) and α is the absorption coefficient of the water (1/m). The absorption can be written as a function of 10-mm transmittance T_{10}:

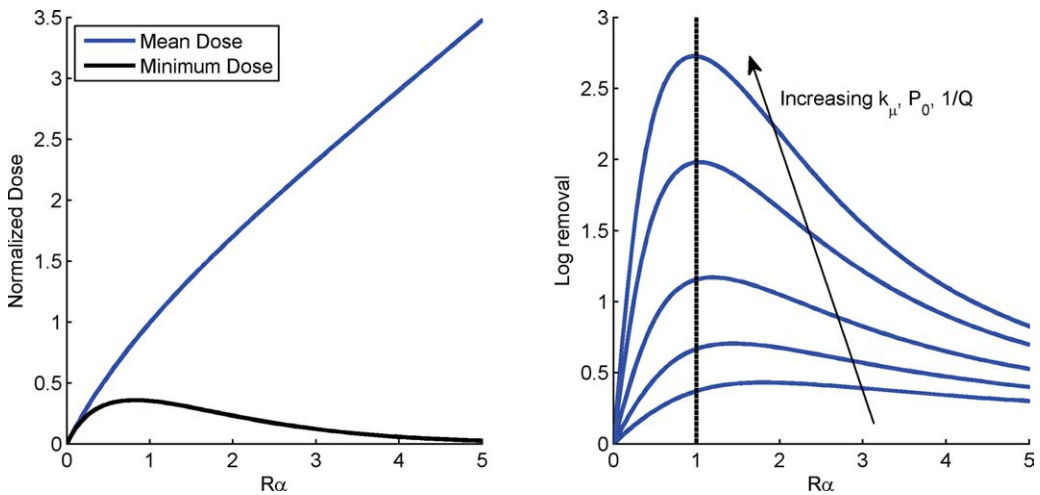

Figure A1. Normalized mean dose and minimal dose as a function of the parameter $R\alpha$ (left).

Log removal as a function of the parameter $R\alpha$ (right). [Color figure can be viewed in the online issue, which is available at wileyonlinelibrary.com.]

$$\alpha = \frac{-\ln(T_{10})}{0.01m} \tag{A3}$$

Assuming a constant velocity profile (with velocities equal to U), the dose distribution is calculated by:

$$D(r) = \frac{I(r)L}{U} = \frac{P_0 V}{2\pi Q} \frac{e^{-\alpha\left(r - r_{\text{lamp}}\right)}}{r}, \tag{A4}$$

where V is the total volume of the reactor, given by $V = L\pi(2r_{\text{lamp}}R + R^2)$, L is the length (in axial direction) of the lamp. By assuming a radius of the reactor equal to $2/\alpha$, at which distance most of the radiation is absorbed, the volume of the reactor reduces to $V = \frac{4\pi L}{\alpha^2}(\alpha r_{\text{lamp}} + 1)$. The characteristic dose is then determined by calculating the dose at $r = 1/\alpha + r_{\text{lamp}}$

$$D_{\text{scale}} = \frac{2P_0 L}{Q\alpha} e^{-1}. \tag{A5}$$

For an arbitrary UV system, the factor P_0L could be replaced by the total lamp power (W).

Optimal distance lamp to outer wall

On the one hand, the distance R from the quartz layer of the lamp to the outer wall must not be too large to prevent areas with small doses due to the small irradiation levels. On the other hand, this distance must not be too small to avoid the loss of radiant energy through the outer walls. Therefore, using a first order Chick–Watson relation, the disinfection is calculated as a function of the parameter $R\alpha$, which contains the distance R and the absorbance. Increasing the parameter $R\alpha$ results in a higher mean dose, because the mean velocity is reduced due to a larger cross-sectional area. But the minimal dose has decreased because the water elements close to the outer wall received less UV radiation (Figure A1). The optimal value of $R\alpha$ depends on the required removal of contaminants. The log removal as a function of $R\alpha$ depends on the inactivation rate k_μ, lamp power P_0, and flow rate Q. For a required log removal between 1 and 3, the optimal distance R is equal to $1/\alpha$. For a T_{10} transmittance of 80%, the optimal distance then becomes $\sim$0.05 m.

Manuscript received Oct. 8, 2009, and revision received Feb. 9, 2010.